AGU PUBLICATIONS

JGR

Journal of Geophysical Research: Atmospheres

RESEARCH ARTICLE
10.1002/2016JD026295

Key Points:
- MODIS AOD and AirNow $PM_{2.5}$ measurements are assimilated into the CMAQ model using an optimal interpolation (OI) method
- MODIS AOD and AirNow $PM_{2.5}$ measurements were first assimilated separately before being assimilated simultaneously over a 30 day period
- Assimilating the total AOD observations is more beneficial for correcting the $PM_{2.5}$ underestimations than directly assimilating $PM_{2.5}$

Correspondence to:
T. Chai,
Tianfeng.Chai@NOAA.gov

Citation:
Chai, T., H.-C. Kim, L. Pan, P. Lee, and D. Tong (2017), Impact of Moderate Resolution Imaging Spectroradiometer Aerosol Optical Depth and AirNow $PM_{2.5}$ assimilation on Community Multi-scale Air Quality aerosol predictions over the contiguous United States, *J. Geophys. Res. Atmos.*, *122*, 5399–5415, doi:10.1002/2016JD026295.

Received 29 NOV 2016
Accepted 30 APR 2017
Accepted article online 2 MAY 2017
Published online 19 MAY 2017

Impact of Moderate Resolution Imaging Spectroradiometer Aerosol Optical Depth and AirNow $PM_{2.5}$ assimilation on Community Multi-scale Air Quality aerosol predictions over the contiguous United States

Tianfeng Chai[1,2], Hyun-Cheol Kim[1,2], Li Pan[1,2], Pius Lee[1], and Daniel Tong[1,2,3]

[1]NOAA Air Resources Laboratory, NOAA Center for Weather and Climate Prediction, College Park, Maryland, USA, [2]Cooperative Institute for Climate and Satellites, University of Maryland, College Park, Maryland, USA, [3]Center for Spatial Information Science and Systems, George Mason University, Fairfax, Virginia, USA

Abstract In this study, Moderate Resolution Imaging Spectroradiometer (MODIS) Aerosol Optical Depth (AOD) and AirNow $PM_{2.5}$ measurements are assimilated into the Community Multi-scale Air Quality (CMAQ) model using an optimal interpolation (OI) method. Over a 30 day test period in July 2011, three assimilation configurations were used in which MODIS AOD and AirNow $PM_{2.5}$ measurements were first assimilated separately before being assimilated simultaneously. The background error covariance is estimated using both the National Meteorological Center approach and the Hollingsworth-Lönnberg method. The AOD observations from Terra are assimilated at 17Z and the Aqua AOD observations are assimilated at 20Z each day. AirNow $PM_{2.5}$ measurements are assimilated 4 times a day at 00Z, 06Z, 12Z, and 18Z. Model performances are measured by the daily averaged and domain-averaged biases and the root-mean-square errors (RMSEs) obtained by comparing the predictions with the AirNow $PM_{2.5}$ observations that were not assimilated. Either assimilating the MODIS AOD or assimilating the AirNow $PM_{2.5}$ alone helps $PM_{2.5}$ predictions over the entire 30 days. The case that assimilates the observations from both sources has the best performance. While the CMAQ $PM_{2.5}$ results exhibit exaggerated diurnal variations compared to the AirNow measurements, this is not as severe at rural sites as at urban or suburban sites. It was also found that assimilating the total AOD observations is more beneficial for correcting the $PM_{2.5}$ underestimations than directly assimilating the AirNow $PM_{2.5}$ measurements every 6 h. While the simple approach of applying the AOD scaling factors uniformly throughout the vertical columns proved effective, it is liable to produce substantial errors. This is demonstrated by a high-AOD event.

1. Introduction

Fine particulate air pollution has been closely monitored worldwide due to its adverse effects, ranging from degraded visibility or haze-fog episodes [*Chow et al.*, 2004; *Sun et al.*, 2006] to the severe cardiovascular and respiratory diseases that it may cause [*Schwartz and Neas*, 2000; *Delfino et al.*, 2005; *Dominici et al.*, 2006]. In order to provide advance notice of future air pollution events, national weather services worldwide are expanding the weather predictions to include air pollution predictions. The U.S. National Air Quality Forecast Capability (NAQFC) provided by the National Oceanic and Atmospheric Administration (NOAA) had its $PM_{2.5}$ (particulate matter with aerodynamic diameter less than or equal to 2.5 μm) predictions using the Community Multi-scale Air Quality (CMAQ) modeling system initially tested in 2006 [*Gorline and Lee*, 2009] and was implemented to operations in 2016 [*Lee et al.*, 2017]. While the aerosol module is being continuously updated, it is still limited by our incomplete understanding of the aerosol chemistry and dynamics. In addition, reliance on often-outdated emission inventories and lack of real-time emission modeling significantly restrict the NAQFC and similar regional aerosol forecast capabilities [*Tong et al.*, 2012].

Continuous efforts have been made to integrate aerosol observations with chemical transport models [*Carmichael et al.*, 2008; *Sandu and Chai*, 2011; *Bocquet et al.*, 2015]. In the U.S. and Canada, hourly $PM_{2.5}$ measurements at surface network stations are usually available at near-real time with high-quality and good spatial coverage. *Kang et al.* [2010a, 2010b] showed promising results in improving $PM_{2.5}$ predictions

using AirNow measurements with a bias-adjustment Kalman Filter technique. *Robichaud and Ménard* [2014] generated multiyear warm season surface $PM_{2.5}$ analyses using the Canadian air quality forecast suite and surface observations based on an optimal interpolation (OI) scheme. In addition to the surface network stations, Moderate Resolution Imaging Spectroradiometers (MODIS) aboard the Terra and Aqua satellites provide near-real-time aerosol optical depth (AOD) observations with good spatial resolution and coverage [*Remer et al.*, 2005]. Assimilating the MODIS AOD proves to be beneficial to aerosol predictions [*Adhikary et al.*, 2008; *Zhang et al.*, 2008; *Liu et al.*, 2011; *Saide et al.*, 2013; *Pagowski et al.*, 2014]. Recently, *Schwartz et al.* [2012] assimilated both MODIS AOD and AirNow $PM_{2.5}$ simultaneously using the National Centers for Environmental Prediction (NCEP) Gridpoint Statistical Interpolation (GSI) three-dimensional variational (3DVAR) data assimilation system with the Weather Research and Forecasting-Chemistry (WRF-Chem) model. They showed that concurrent assimilation of $PM_{2.5}$ and AOD observations produced the best overall forecasts.

In this study, an OI scheme is used to assimilate the AirNow $PM_{2.5}$ and MODIS AOD measurements into the NAQFC system which employs the CMAQ model. The impact of the assimilation is objectively assessed by using the observations that are not assimilated or before they are assimilated. *Tang et al.* [2015] presented a case study using the same OI data assimilation package with some modifications to assimilate AirNow ozone, $PM_{2.5}$, and MODIS AOD measurements. This paper focuses on $PM_{2.5}$ only and provides more details on the method. While *Tang et al.* [2015] designed four different OI cases to examine the effects of different uncertainty setting and assimilation time, this paper tries to compare the effects of $PM_{2.5}$ and MODIS AOD measurements in the data assimilation. Some differences between the two implementations will be presented and discussed in the following sections. It is also noted that the outdated emission inventories are not updated here. Thus, the prediction errors due to emissions will persist and the data assimilation effects could decay quickly. Assimilating satellite data to constrain the aerosol sources has proved quite successful in various applications [e.g., *Chai et al.*, 2009; *Kaiser et al.*, 2012; *Xu et al.*, 2013; *Zhang et al.*, 2015; *Wang et al.*, 2016; *Chai et al.*, 2017]. Including top-down emission inversion to improve the $PM_{2.5}$ predictions will be explored in the future.

The remainder of the paper is organized as follows. The assimilation system is explained in section 2. It includes a brief description of the NAQFC-β system, the AirNow and MODIS observations, the OI method, and the setup of the assimilation tests. Detailed model results are presented in section 3, and section 4 provides a summary and some discussion.

2. Description of the Assimilation System

2.1. NAQFC-β System

The experimental version of the NAQFC system (NAQFC-β) used in this study is composed of a CMAQ modeling system [*Byun and Schere*, 2006] driven by the NCEP's North American Mesoscale (NAM) meteorological forecasts with the Weather Research and Forecasting (WRF) Nonhydrostatic Mesoscale Model (NMM) core [*Janjic*, 2003]. A preprocessor to CMAQ, PREMAQ prepares the CMAQ input files after taking in the WRF postprocessor outputs [*Otte et al.*, 2005]. The system is identical to the Base Case described in *Pan et al.* [2014], using CMAQ version 4.7.1 with the AERO-5 aerosol module [*Carlton et al.*, 2010] and online biogenic emissions (BEI3.13) [*Schwede et al.*, 2005].

Figure 1 shows the computational domain, which is covered by a 442 × 265 grid with a 12 km horizontal resolution following a Lambert conformal conic (LCC) projection. There are 22 vertical layers extending from the surface to 100 hPa, with a hybrid pressure/sigma coordinate that is the same as that of the WRF-NMM model (see *Lee and Ngan* [2011] for details). A zero-flux assumption at the top boundary is made in the CMAQ computation. The other details of the NAQFC-β system can be found in earlier publications [*Chai et al.*, 2013; *Pan et al.*, 2014].

2.2. MODIS AOD Observations

Level-2 MODIS AOD at 550 nm from Collection 051 with the best quality (Quality flag = 3) are used in this study [*Levy et al.*, 2009]. They include both ocean and land products (MOD04 and MYD04) with up to 10 × 10 km horizontal resolution from Terra and Aqua platforms, which pass over the equator at around 10:30 and 13:30 LT, respectively. The total AOD is read from the database and then regridded into the target domain. The average AOD values of the pixels inside each grid cell are taken as the observation input to be compared with their model equivalents.

Zhang and Reid [2006] and *Hyer et al.* [2011] evaluated the MODIS Collection 5 optical depth retrievals and developed an empirical quality control and assurance procedure to filter and correct the AOD data. However,

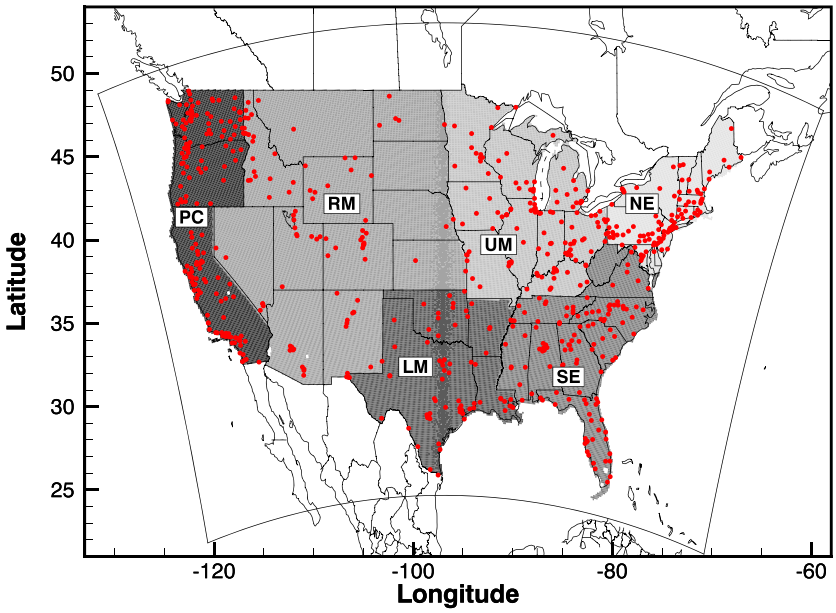

Figure 1. The NAQFC computational domain and the six predefined U.S. regions, i.e., Pacific Coast (PC), Rocky Mountain (RM), Southeast (SE), Lower Middle (LM), Upper Middle (UM), and Northeast (NE). The 672 AirNow stations that reported $PM_{2.5}$ measurements over the contiguous United States (CONUS) are also marked.

such extra screening and correction might not be critical for the Collection 6 MODIS aerosol products which had changes to both "upstream" and retrieval algorithms albeit not a major overhaul [*Levy et al.*, 2013]. In this study, the MODIS AOD data from Collection 051 were used, similar as in *Tang et al.* [2015]. A comparison of the July 2011 AOD data in our computational domain between the Collection 051 and the Collection 6 shows good agreement and no severe bias, with the linear regression slopes of Collection 6 over Collection 051 as 1.01 and 0.98 for Terra and Aqua, respectively. In addition, both the Collection 051 and the Collection 6 AOD data are compared with the collocated AOD data from 77 AERONET sites at 0.5 μm [*Holben et al.*, 1998] for the entire month. The Collection 6 data yield a better correlation with the AERONET data ($r = 0.91$) than the Collection 5.1 data ($r = 0.79$). However, the Collection 6 data show a higher mean bias (0.03) than the Collection 5.1 data (−0.01) when compared with the AERONET AOD data. *Drury et al.* [2008] and *Wang et al.* [2010] presented improved algorithms for MODIS satellite retrievals of AODs. Nonetheless, the Collection 6 MODIS data will be used in the future and necessary quality assurance and quality control procedure should be applied as well.

Note that the MODIS AOD fine-mode fraction parameters can be applied to the original total AOD to get fine-mode AOD values. However, spatial coverage decreases as the fine-mode fraction parameters are not always available. *Chai et al.* [2014] demonstrated that assimilating the total AOD performs better than assimilating the fine-mode AOD. Only total AOD values are used in the following tests in this paper.

The CMAQ counterparts of the total AOD are calculated by integrating the hourly extinction coefficients over the whole vertical columns. In CMAQ, the extinction coefficients can be calculated from the Mie theory or using the mass reconstruction method [*Mebust et al.*, 2003]. The AOD results from the two methods are quite similar. We chose to use the mass reconstruction method.

2.3. AirNow $PM_{2.5}$ Measurements

Near-real-time ozone and $PM_{2.5}$ measurements are provided by the U.S. EPA AirNow program (http://airnowapi.org). The measurements then go through quality control and assurance and are made available through the Air Quality System (AQS) but at a much later time. Since improving $PM_{2.5}$ forecasts is a major goal here, the AQS data are not suitable here due to their late availability. Figure 1 shows the distribution of the 672 AirNow stations that reported $PM_{2.5}$ measurements over the contiguous United States (CONUS) in July 2011. When comparing model predictions with AirNow $PM_{2.5}$ observations, the aerosol components of Aitken and accumulation modes at the monitor-residing grid cells were added to construct the CMAQ $PM_{2.5}$. While 672 AirNow stations reside in 632 grid cells, 28 grid cells have two to five monitors in them. During the

assimilation, only one measurement is used without preference for grid cells where there are two or more valid observations. However, all the measurements are compared against the model predictions when calculating the model performance statistics.

2.4. Optimal Interpolation

A simple data assimilation scheme, optimal interpolation (OI), is chosen to assimilate observations into the CMAQ chemical transport model (CTM). In OI, analysis is obtained by directly solving equation (1),

$$\boldsymbol{X}^a = \boldsymbol{X}^b + \boldsymbol{BH}^T \left(\boldsymbol{HBH}^T + \boldsymbol{O}\right)^{-1} \left(\boldsymbol{Y} - \boldsymbol{HX}^b\right), \tag{1}$$

where $\boldsymbol{X}$ and $\boldsymbol{Y}$ are state and observation vectors, respectively. B and O are background and observation error-covariance matrices. H is a linearized observational operator. Superscripts a and b indicate analysis and background states, respectively. Observations beyond the background-error correlation length scale have no effect in the analysis.

Rather than directly solving equation (1), we choose to apply the optimal interpolation (OI) in an alternative format,

$$\boldsymbol{H'X}^a = \boldsymbol{H'X}^b + \boldsymbol{H'BH}^T \left(\boldsymbol{HBH}^T + \boldsymbol{O}\right)^{-1} \left(\boldsymbol{Y} - \boldsymbol{HX}^b\right). \tag{2}$$

With $\boldsymbol{H'}$ representing transformation of variable for τ (AOD) or $PM_{2.5}$ for the whole domain, $\boldsymbol{H'X}^a$ and $\boldsymbol{H'X}^b$ can be written as $\boldsymbol{\tau}^a$ and $\boldsymbol{\tau}^b$ or $\mathbf{PM}^a_{2.5}$ and $\mathbf{PM}^b_{2.5}$. $\boldsymbol{HBH}^T$ becomes background error statistics for τ or $\mathbf{PM}_{2.5}$ at observation locations. While the MODIS observation time can vary up to 5 h between the East Coast and the West Coast, the daily data are assimilated at the approximate midpoints of the daily scanning over the CONUS, at 17Z for Terra and at 20Z for Aqua. This is mainly to reduce the frequency of analysis operation when the model has to stop to inject data. *Schwartz et al.* [2012] assimilated AOD data at 18Z and 0Z using data within 3 h for a similar CONUS domain. *Tang et al.* [2015] assimilated the Terra and Aqua data over the CONUS domain at 17Z and 19Z, respectively. The $\frac{\tau^a}{\tau^b}$ at each grid point is used to scale all aerosol components throughout the vertical column. It implies zero background error for the ratio between any speciated aerosol components at each grid point and zero background error for the ratio of τ or $PM_{2.5}$ between any two vertical levels at any location. Such simplification is due to the lack of information to constrain speciated aerosol components or their vertical distribution. When AirNow $PM_{2.5}$ measurements are assimilated, the hourly measurements at 00Z, 06Z, 12Z, and 18Z will be input into equation (1) to generate the new analysis fields. As the measurements are made at the surface, the scaling factors $\frac{PM^a_{2.5}}{PM^b_{2.5}}$ only apply to the levels below the boundary layer top. Whenever observations are assimilated, the state variables that comprise the aerosol in the model are adjusted from their background to their analysis states using the scaling factors obtained following equation (2).

After assimilating the AOD or $PM_{2.5}$ observations, the adjusted model state variables are then used to initiate the CMAQ model to predict the next background state $\boldsymbol{X}^b$ in equation (1). In future real-time implementations, the subsequent model simulation can be extended over a longer period in order to generate future forecasts. As the forward prediction is indeed "hindcast" in this study, the term "prediction" instead of "forecast" is used here to indicate the characteristics of the "free" runs that do not assimilate observations along the way. Note that the background state $\boldsymbol{X}^b$ is actually a "prediction" of the previous model run before it is combined with the newly available observation $\boldsymbol{Y}$ to generate a new analysis state $\boldsymbol{X}^a$ using equation (1).

2.5. Error Statistics

The AOD background error statistics are estimated using both the National Meteorological Center (NMC) approach and the Hollingsworth-Lönnberg (observational) method, following *Chai et al.* [2007]. In the NMC approach, 24 h average τ from 13Z 16 August to 12Z 17 August 2001 are calculated over the entire model domain using two NAQFC CMAQ runs that were driven by two meteorological forecast fields which started 24 h apart. The differences between the two meteorological fields are caused by the assimilation of additional 24 h meteorological observations in the later run. The AOD differences are calculated at all geolocations and are used as surrogates for model errors in the NMC approach in order to calculate the error statistics. In Hollingsworth-Lönnberg method, the actual differences between the model predictions and the measurements are calculated. In this observation-based procedure, the regridded AOD measurements are treated as measurements from imaginary stations located at the center of each grid cell. The AOD observations are collected from the Terra data from the 14–20 August 2009 period. The corresponding CMAQ τ predictions are calculated using the mass reconstruction method based on the experimental NAQFC runs which had no AOD or PM2.5 assimilation. The "station pairs" with valid observation pairs for more than 2 days are used to calculate the covariance between the "stations." Note that the biases need to be removed before calculating

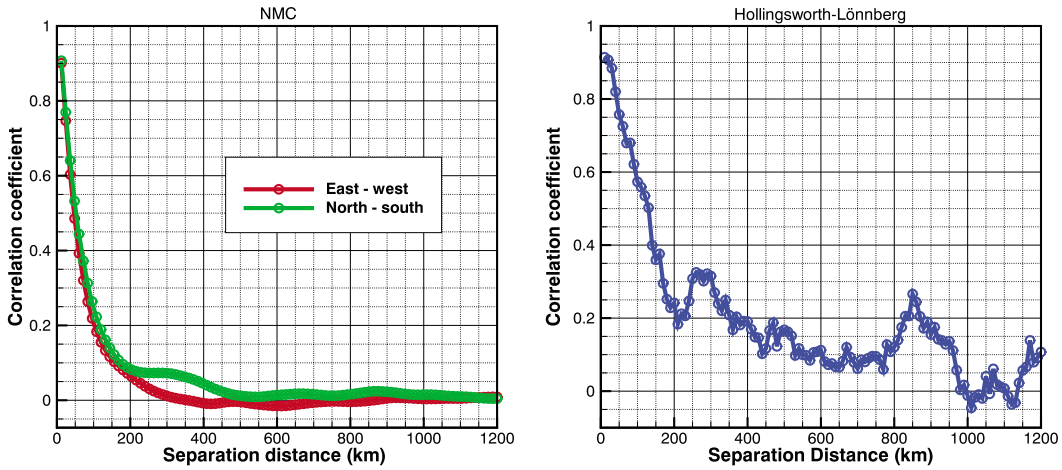

Figure 2. The average correlation coefficient as a function of separation distance between two grid cells for AOD from the NMC approach and the Hollingsworth-Lönnberg method, respectively.

the covariance. Although the error statistics are more realistic, the method is limited by the availability of observations.

To avoid storing the background error covariance matrix $\boldsymbol{B}$, the background error covariance between any two geolocations P_i and P_j is modeled as

$$\mathrm{COV}_{ij} = \epsilon_i \epsilon_j e^{-\frac{\Delta_{ij}}{l_h}} \tag{3}$$

where ϵ_i and ϵ_j are the standard deviations of the background errors, which are assumed to be unbiased. The Δ_{ij} is the distance between the two geolocations P_i and P_j, l_h is the horizontal correlation length scale parameter to be estimated, and l_h can be estimated using either of the two methods described above. For simplicity, the background error correlation coefficients are assumed to be homogeneous and isotropic, and they are further assumed to be stationary. However, the variation of ϵ from point to point makes the background error covariance inhomogeneous.

Figure 2 shows the average correlation coefficient, i.e., $\frac{\mathrm{COV}_{ij}}{\epsilon_i \cdot \epsilon_j}$, as a function of the separation distance between two grid cells from the NMC approach and the Hollingsworth-Lönnberg method, respectively. The results from the Hollingsworth-Lönnberg method are averaged over 10 km bins. In the NMC approach, the pairings are restricted to the stations along the same longitude and latitude of the computational grid, denoted as "East-west" and "North-south," respectively, in Figure 2. This effectively reduces the number of valid "station pairs" from $\sim 6.86 \times 10^9$ to $\sim 2.58 \times 10^7$ and $\sim 1.55 \times 10^7$ for East-west and North-south pairings, respectively, compared to 13605 valid pairs in the Hollingsworth-Lönnberg method. The large quantity of samples available in the NMC approach results in much smoother curves than achieved in the Hollingsworth-Lönnberg method. The close resemblance of the East-west and North-south results partially validates the earlier isotropic assumption. The NMC results show a correlation length scale of ~84 km, which is the separation distance where the corresponding correlation coefficient falls to e^{-1}. However, the Hollingsworth-Lönnberg method indicates a longer correlation length scale of ~160 km. The vertical intercept $R_z \approx 0.92$ at $\Delta_{ij} = 0$ for the observational method in Figure 2 indicates that the background error is much greater than the observational error.

Using the AirNow hourly $PM_{2.5}$ measurements from July 2011 and the NAQFC CMAQ predictions, the Hollingsworth-Lönnberg method is applied within the six CONUS regions defined in Figure 1. Figure 3 shows the correlation coefficients averaged over 10 km bins. The Lower Middle (LM) region shows the largest correlation length, and the Rocky Mountain (RM) region has the shortest correlation length. The curves for the other four regions fall in between these. They are mostly clustered together and show a length close to 100 km. In the following assimilation tests, we chose $l_h = 84$ km for both AOD and $PM_{2.5}$. Such a conservative choice tends to limit the effective radius of each individual observation. In addition, the standard deviation of the background errors is assigned as 60% of the background values, while the observational errors are assumed to be $\pm 0.04 \pm 0.20\tau$ for AOD and ±20% of the measurement values for $PM_{2.5}$. Although the AOD retrievals over

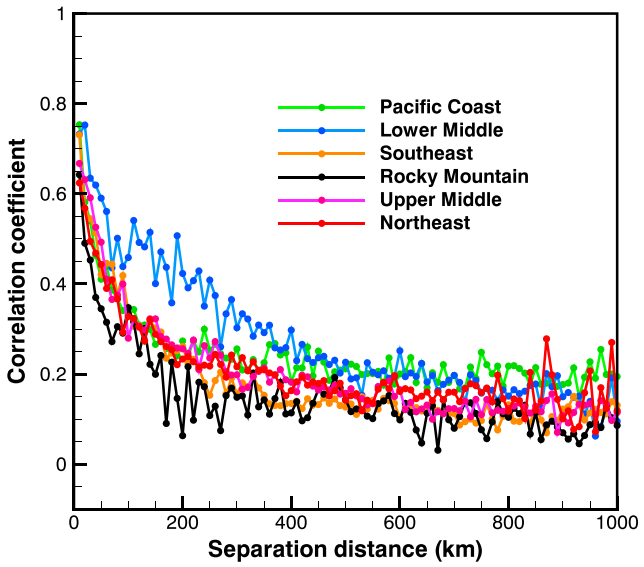

Figure 3. The average correlation coefficient as a function of separation distance between two stations for $PM_{2.5}$ using the Hollingsworth-Lönnberg method.

ocean were shown with less uncertainties ($\Delta\tau = \pm 0.03 \pm 0.05\tau$) than those over the land ($\Delta\tau = \pm 0.05 \pm 0.15\tau$) [*Remer et al.*, 2005], for simplicity, the assumed $\Delta\tau = \pm 0.04 \pm 0.20\tau$ uncertainties are applied to all the AOD data. Note that the observational errors here include representative errors besides the uncertainties of the AOD retrievals. Although the AirNow $PM_{2.5}$ measurement errors are much smaller than those of the MODIS τ retrievals, comparing the in situ point measurements with grid average concentrations results in larger representative errors for AirNow $PM_{2.5}$.

3. Results

3.1. Assimilation Tests

As listed in Table 1, two assimilation configurations, C1 and C2, were designed to assimilate the AOD and $PM_{2.5}$ observations separately. Then both the AOD and $PM_{2.5}$ observations are assimilated in configuration C3. A baseline case without any assimilation is also included in order to evaluate the effect of assimilation. All configurations start at 12Z on 1 July 2011. They then assimilate the observations at designated instants, running until 12Z on 31 July 2011. In the three assimilation tests, adjusted initial states are used to run the model after each assimilation instant. The longest "free" run period is 21 h for C2 between assimilating Aqua AOD and assimilating the Terra AOD of the next day.

Figure 4 shows the $PM_{2.5}$ predictions from the baseline case (C0) and the three assimilation tests (C1 – C3). Note that Figure 4 shows $PM_{2.5}$ at every hour even though C2 and C3 only assimilate the observations at 00Z, 06Z, 12Z, and 18Z. As mentioned earlier, there are two state vectors available at the instants when OI is performed: (1) the background, that is, the "forecasts" of the previous model run and (2) the "analysis" that results from integrating the observations with the background states. The "forecast" results are used in Figure 4 and in all other evaluations, unless otherwise specified. The baseline case significantly underestimates $PM_{2.5}$ over the entire period. Such underestimation of $PM_{2.5}$ over the CONUS by the CMAQ model during the summer months has been well documented [*Morris et al.*, 2005a, 2005b; *Luo et al.*, 2011; *Baek et al.*, 2011; *Xing et al.*, 2015]. Using SO_4^{2-}, NO_3^-, NH_4^+, and EC observations from 1990 to 2010 by the U.S. CASTNET and IMPROVE networks, *Xing et al.* [2015] reported that the CMAQ simulation significantly underestimated all aerosol species in summer over that 20 year period, with the normalized mean bias ranging from −28.9% to −73.5%. Assimilating either MODIS AOD or $PM_{2.5}$ helps $PM_{2.5}$ predictions over the entire 30 days. Figure 4 shows that the three assimilation tests were able to mitigate the underestimation, resulting in much better matching between the model predictions and the AirNow observations than in the C0 case. The fact that assimilating AOD data is more effective than assimilating AirNow observations is due to the much better spatial coverage of the satellite than the ground stations which only occupy 0.54% of the grid cells at the surface. As a result, it also retains the analysis information better. *Chai et al.* [2014] showed that the assimilation effect can be seen after 24 h

Table 1. Observations Assimilated at Designated Times for the Test Cases

Cases	12Z	17Z	18Z	20Z	00Z[a]	06Z[a]
C0	-	-	-	-	-	-
C1	-	Terra total AOD	-	Aqua total AOD	-	-
C2	$PM_{2.5}$	-	$PM_{2.5}$	-	$PM_{2.5}$	$PM_{2.5}$
C3	$PM_{2.5}$	Terra total AOD	$PM_{2.5}$	Aqua total AOD	$PM_{2.5}$	$PM_{2.5}$

[a]Denotes the next day.

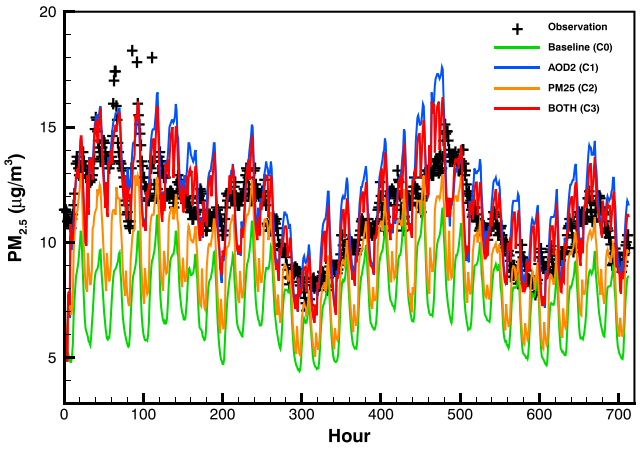

Figure 4. Time series of domain-averaged $PM_{2.5}$. Hour number counting starts from 12Z on 1 July 2011. Hour 14 is not plotted here as only seven valid observations are available at the hour. The cutoff $PM_{2.5}$ observations at hours 87–91 are 24.6, 29.1, 32.3, 25.0, and 20.6 μg/m^3, respectively.

of the assimilation when only Terra AOD data were assimilated. Configuration C3, in which observations are assimilated from both sources, achieves the best results. Also note that the effects of the Independence Day fireworks are shown by the observations but are not reflected in any of the CMAQ tests. *Seidel and Birnbaum* [2015] demonstrated the similar effects using the AQS $PM_{2.5}$ data from 1999 to 2013 and suggested future inclusion in the model of the fireworks celebrating the 4 July as emission sources.

Figure 4 also shows that the model demonstrates significant diurnal patterns, which were not observed at AirNow stations. Such exaggerated diurnal variability in the CMAQ model has been reported in other studies [*Morris et al.*, 2006; *McKeen et al.*, 2007; *Djalalova et al.*, 2015]. *McKeen et al.* [2007] showed that the CMAQ model failed to capture an observed $PM_{2.5}$ decrease from 0100 to 0600 LT and speculated that its failure indicated that the model underrepresented the aerosol loss during the late night and early morning hours. Figure 5 shows a very similar pattern in the baseline case C0. The $PM_{2.5}$ measurements by the AirNow stations show a steady decrease from 0000 to 0500 LT, but the CMAQ results in case C0 show the opposite trend, namely, a steady increase from 0000 to 0500 LT. The model results also exhibit a significant underestimation during the afternoon hours, which is speculated to be related to the underprediction of secondary production for organic carbon in CMAQ [*Doraiswamy et al.*, 2010; *Baek et al.*, 2011]. Such systematic errors are not considered in the current bias-blind data assimilation scheme. Bias-aware assimilation methods can be designed to estimate and correct the model biases [*Dee and Da Silva*, 1998; *Dee*, 2005].

Using the local settings of the AirNow stations, domain-averaged hourly $PM_{2.5}$ at urban, suburban, and rural sites are calculated and shown in Figure 6. The time series at the urban and suburban sites are similar, resembling what is shown in Figure 4 for all stations. The rural sites are associated with lower $PM_{2.5}$ and display much smaller diurnal variation. When both MODIS AOD and AirNow $PM_{2.5}$ are assimilated, Figure 6 shows that the CMAQ model captures the mean $PM_{2.5}$ at rural sites extremely well. It is noticed that the diurnal variability at rural sites is not as excessive as that at urban or suburban sites. This may indicate problems with the diurnal profiles of the sources associated with the urban and suburban settings, such as mobile emission sources related to local traffic. However, it might also be related to the planetary boundary layer (PBL) height or removal processes. Further investigation is required to identify the cause of the exaggerated diurnal variability displayed by the model. To prevent the diurnal patterns from playing too much

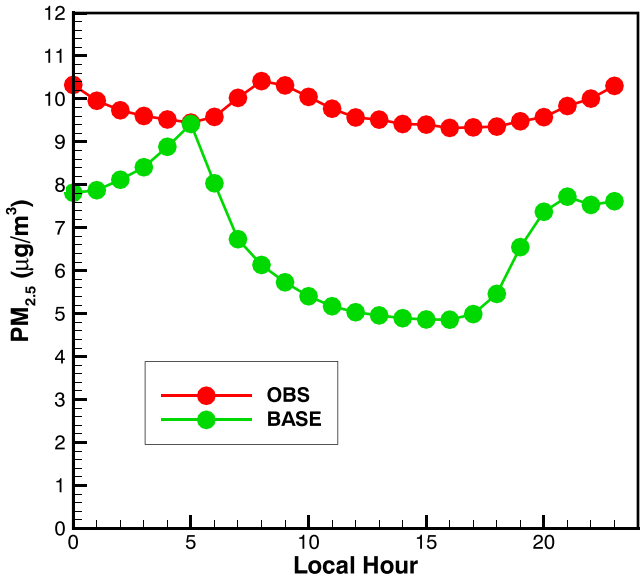

Figure 5. $PM_{2.5}$ of case C0 at local hours, averaged from 12Z on 1 July to 11Z on 31 July 2011. OBS: AirNow measurements; BASE: CMAQ results of Case C0.

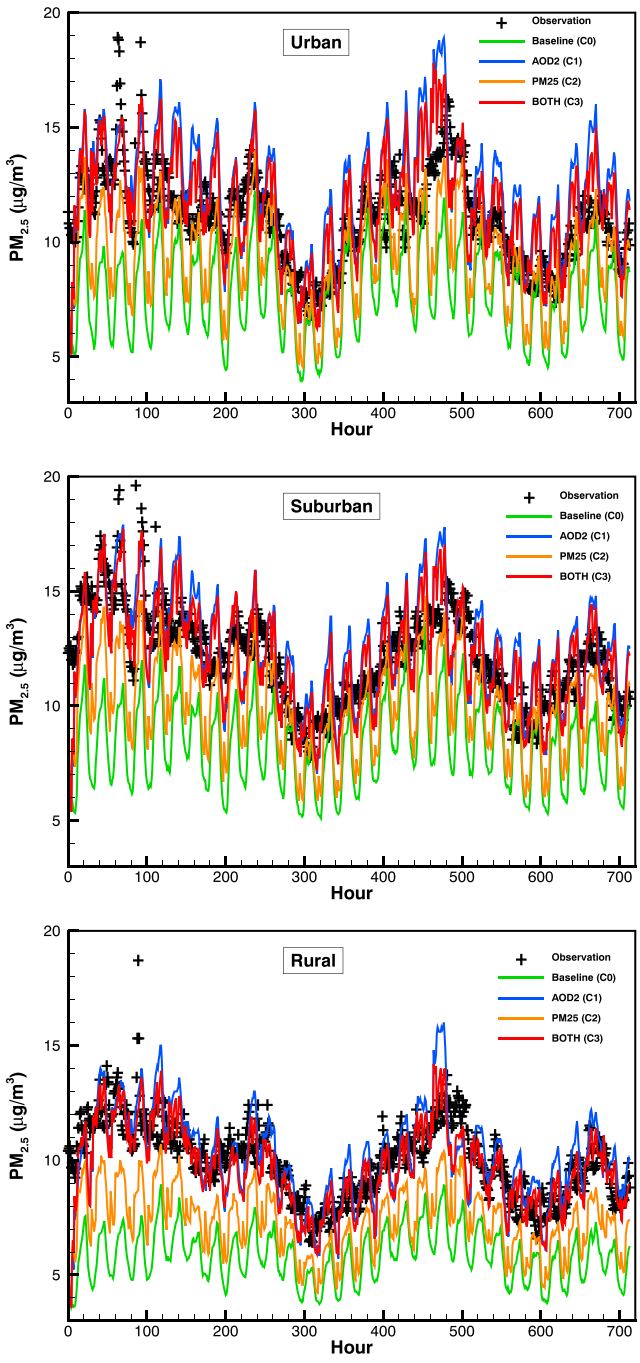

Figure 6. Time series of mean domain-averaged hourly $PM_{2.5}$ at urban, suburban, and rural AirNow sites. Hour number counting starts from 12Z on 1 July 2011. Hour 14 is not plotted here as only seven valid observations are available at the hour. Observations above 20 μg/m^3 at hours 86–91 for urban sites and at hours 87–91 for suburban sites are cut off from the plots.

a role, the error statistics listed in Tables 2–3 are based on the 24 h average $PM_{2.5}$ calculated from 12Z to 11Z to the next day. Note that 24 h average $PM_{2.5}$ is also associated with the past and current National Ambient Air Quality Standards in the United States.

Table 2 shows the evaluation statistics for 24 h average $PM_{2.5}$ at all AirNow sites as well as for urban, suburban, and rural settings separately. For the test period, the suburban sites had the highest mean observed $PM_{2.5}$ at 12.3 μg/m^3, while the rural sites had the lowest mean observation, at 10.0 μg/m^3. Overall, the baseline case C0 significantly underestimates $PM_{2.5}$ regardless of the local settings of the stations. Among stations with different local settings, Case C0 has the largest bias at rural sites (−4.2 μg/m^3), which may be clearly seen in Figure 6. After integrating the MODIS AOD observations, case C1 reverses the significant underestimation into a slight overestimation, resulting in mean biases ranging from 0.2 μg/m^3 at both suburban and rural sites to 0.9 μg/m^3 at urban sites. Case C2, which assimilates AirNow $PM_{2.5}$ alone, still underestimates $PM_{2.5}$, but the magnitudes of the underestimation are cut by more than a third for all three sets of the AirNow stations. In Table 2, the $PM_{2.5}$ root-mean-square error (RMSE) shows that C2 performs better than C1. Note that only $PM_{2.5}$ observations at 00Z, 06Z, 12Z, and 18Z are assimilated in C2 and C3; the evaluations are based on 24 h average $PM_{2.5}$ calculated over all hours. In addition, the "forecast" values rather than the "analyses" at the integration times are used in calculating the evaluation statistics. Although assimilating τ significantly improves the $PM_{2.5}$ model bias, the simple treatment of applying τ scaling factors to all aerosol components over a whole column cannot avoid inadvertently adjusting surface $PM_{2.5}$ even though MODIS AOD measurements may only reflect aerosols at higher levels. When both MODIS AOD and AirNow surface $PM_{2.5}$ are assimilated in C3, the RMSEs are further improved from C2, resulting in more than 20% reduction compared to the baseline case C0 whether all stations or any of the separate sets of stations are used. Calculated with all stations, the 24 h average $PM_{2.5}$ bias reaches a minimal value of −0.1 μg/m^3, indicating the benefit of combining observations from space and surface stations.

Table 2. Evaluation Statistics of 24 h Average $PM_{2.5}$ at All Airnow Sites As Well As in Urban, Suburban, and Rural Settings Separately[a]

	Mean (μg/m^3)					Bias (μg/m^3)				RMSE (μg/m^3)				
Local Setting	OBS	C0	C1	C2	C3	C0	C1	C2	C3	C0	C1	C2	C3	N
All	11.4	7.5	11.8	9.0	11.3	−3.8	0.4	−2.4	−0.1	6.9	6.3	5.6	5.1	19,149
Urban	11.3	7.9	12.2	9.2	11.7	−3.4	0.9	−2.1	0.4	6.6	6.4	5.5	5.2	6,137
Suburban	12.3	8.4	12.6	9.9	12.2	−3.9	0.2	−2.4	−0.2	7.2	6.5	5.9	5.4	7,877
Rural	10.0	5.8	10.1	7.2	9.6	−4.2	0.2	−2.8	−0.4	6.7	5.8	5.3	4.6	5,059

[a]OBS: AirNow observations; RMSE: root-mean-square error; N: number of data pairs. The 24 h average $PM_{2.5}$ is calculated from 12Z to 11Z to the next day. Note that the total data pairs here do not add up to 19,149, since several AirNow monitoring sites have an unknown category.

Figure 7 shows the time series of the mean 24 h averaged $PM_{2.5}$ in the six predefined U.S. regions shown in Figure 1: the Pacific Coast, Rocky Mountain, Southeast, Lower Middle, Upper Middle, and Northeast. The evaluation statistics for the six regions are listed in Table 3. Underestimation happens in all regions over the whole time period. It is most severe in the Southeast region, with a mean bias of −4.8 μg/m^3. If normalized by the regional mean observation, the Rocky Mountain region has the worst relative bias, −43%. In spite of these large biases, daily variations are mostly captured, as in the Southeast and Northeast regions. When comparing results from the four cases, Figure 7 shows that the regional results agree with the overall feature observed earlier for the CONUS results. Assimilating MODIS AOD alone, case C1, tends to overadjust and reverse the underestimation into an overestimation of $PM_{2.5}$. In four of the six regions, C1 results in a positive $PM_{2.5}$ bias. Only case C2, assimilating AirNow $PM_{2.5}$ observations, mitigates the severe underestimation in all the regions, but it still ends up with significant underestimation. In five of the six regions, C2 has smaller mean RMSEs than does C1, as evaluated by the 24 h averaged $PM_{2.5}$ measurements. Except for the Lower Middle region, C1 results in smaller RMSEs than the baseline case after assimilating the MODIS AOD alone. When both the MODIS AOD and AirNow observations are assimilated, C3 generates the best results, as measured by both the mean bias and the RMSE.

The two days in Figure 7, 8 and 20 July 2011, are chosen to show how assimilating MODIS AOD and AirNow observations affects the CMAQ simulation of $PM_{2.5}$. On 8 July, with MODIS AOD assimilated, cases C1 and C3 agree much better with the observations than does the baseline case C0 or case C2 which only assimilates AirNow measurements. On 20 July, cases C1 and C3 significantly overestimate the $PM_{2.5}$ in the Northeast region. Assimilated Terra and Aqua AOD observations for both days and for 1 day prior are shown in Figure 8. Figure 9 shows the $PM_{2.5}$ measurements at 06Z and 12Z on these two days, along with the $PM_{2.5}$ results from the baseline case C0. Although the AOD observations have gaps in coverage, they cover many more grid cells than the AirNow stations. Figures 10 and 11 show the simulated AOD at 17Z and $PM_{2.5}$ at 18Z for cases C0–C3, on 8 and 20 July, respectively. It is apparent that the spatial patterns of the simulated AOD at 17Z and $PM_{2.5}$ at 18Z are highly correlated. For both days, the baseline case shows the lowest simulated AOD and $PM_{2.5}$.

Table 3. Evaluation Statistics of 24 h Average $PM_{2.5}$ in the CONUS and the Six Predefined U.S. Regions Shown in Figure 1[a]

	Mean (μg/m^3)					Bias (μg/m^3)				RMSE (μg/m^3)				
Region	OBS	C0	C1	C2	C3	C0	C1	C2	C3	C0	C1	C2	C3	N
PC	7.6	4.5	8.4	5.5	7.7	−3.1	0.9	−2.1	0.1	5.8	5.0	4.6	3.9	4627
LM	10.4	6.0	9.1	7.3	9.3	−4.4	−1.3	−3.2	−1.2	6.3	5.0	5.1	4.3	2029
SE	13.7	8.9	13.8	11.0	13.5	−4.8	0.2	−2.7	−0.2	7.5	6.1	5.6	4.9	3437
RM	7.4	4.2	9.9	5.0	8.4	−3.2	2.5	−2.3	1.1	6.1	6.7	5.5	5.2	2698
UM	15.6	11.7	14.6	13.5	14.9	−3.9	−0.9	−2.0	−0.7	8.4	7.7	7.0	6.7	3407
NE	14.1	10.1	14.9	11.7	14.4	−3.9	0.9	−2.4	0.3	7.0	6.8	5.4	5.4	2951

[a]Pacific Coast (PC), Rocky Mountain (RM), Southeast (SE), Lower Middle (LM), Upper Middle (UM), and Northeast (NE); OBS: AirNow observations; RMSE: root-mean-square error; N: number of data pairs. The 24 h average $PM_{2.5}$ is calculated from 12Z to 11Z to the next day.

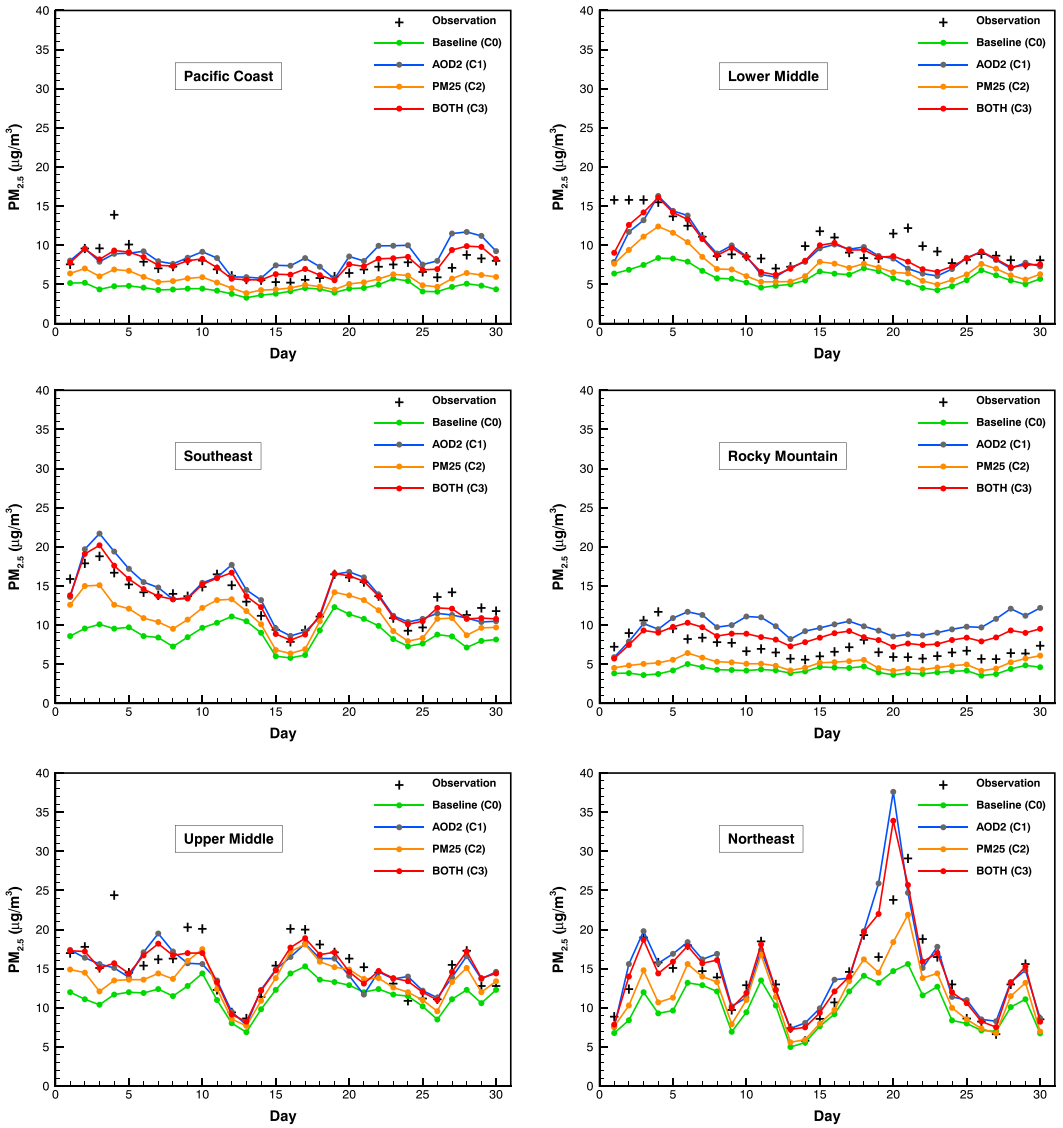

Figure 7. Time series of mean 24 h averaged $PM_{2.5}$ in the six predefined U.S. regions shown in Figure 1, i.e., Pacific Coast (PC), Rocky Mountain (RM), Southeast (SE), Lower Middle (LM), Upper Middle (UM), and Northeast (NE). The 24 h average $PM_{2.5}$ is calculated from 12Z to 11Z to the next day.

Case C2, with AirNow $PM_{2.5}$ observations assimilated 4 times a day, shows elevated levels of both AOD and $PM_{2.5}$, while cases C1 and C3 have much higher AOD and $PM_{2.5}$ after the MODIS AOD retrievals are assimilated twice a day.

On 8 July, the baseline case underestimates surface $PM_{2.5}$ at almost all stations. After assimilating AOD observations, C1 has $PM_{2.5}$ agreeing well with the observations at most stations. This is particularly true in the Southeast region where several high $PM_{2.5}$ measurements are well captured. Figure 8 shows that both Terra and Aqua recorded high AOD values in Georgia and South Carolina on 7 July. On 8 July, although valid AOD observations in the region are limited, high AODs can still be seen in the same area. Note that the Aqua AODs on 8 July have no effect on $PM_{2.5}$ at 18Z on 8 July and they are only shown as references. In the Northeast region, C1 has much higher simulated AOD values as well as elevated $PM_{2.5}$ values. However, several high $PM_{2.5}$ measurements in the southeast Pennsylvania, Maryland, and New Jersey area are not predicted by the model. These high $PM_{2.5}$ measurements are also interspersed with several medium-level measurements. It is extremely difficult to capture such spatial variability using the current model at 12 km resolution. Figure 8 shows that the AOD observations in the area have gaps and the recorded AOD values are not as high as those in the Southeast area. Case C2 shows slightly improved $PM_{2.5}$ at most stations. However, the changes after

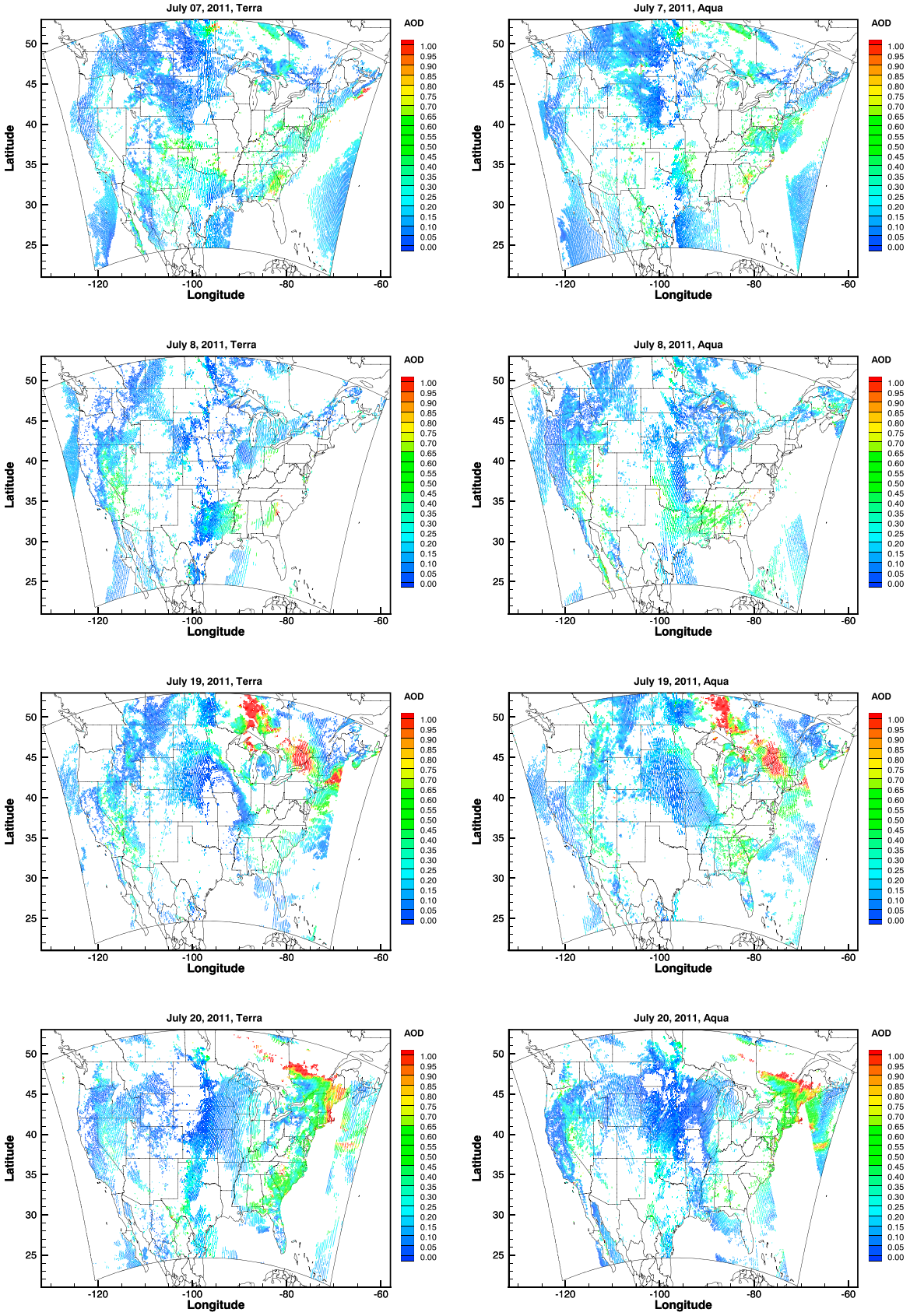

Figure 8. MODIS AOD on 7, 8, 19, and 20 July 2011. Both (left column) Terra and (right column) Aqua are shown.

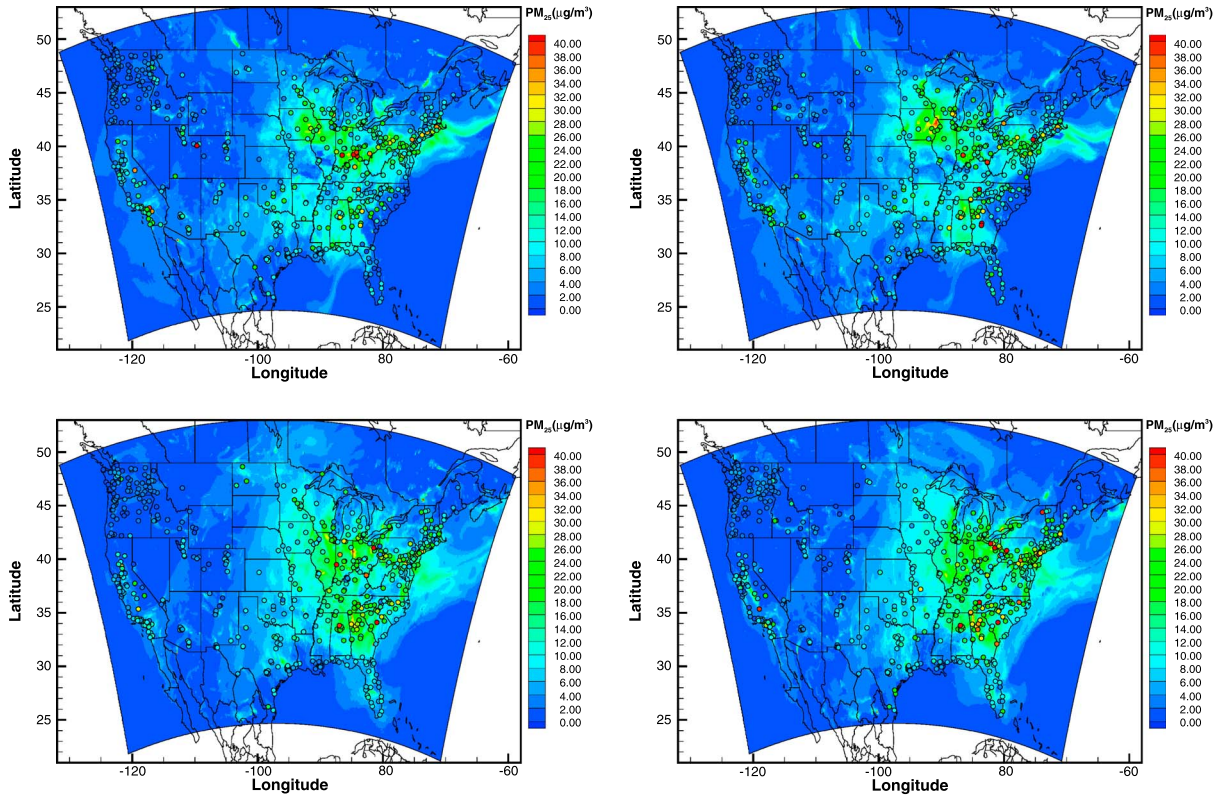

Figure 9. AirNow observations at (left column) 6Z and (right column) 12Z on (top row) 8 July and (bottom row) 20 July. CMAQ $PM_{2.5}$ of the baseline case C0 is also shown.

assimilating $PM_{2.5}$ observations are modest compared to the results of integrating AOD observations in C1. The latest observation inputs that affect the $PM_{2.5}$ at 18Z on 8 July are at 6Z and 12Z on the same day, shown in Figure 9. These appear to be quite different from the $PM_{2.5}$ at 18Z, especially for high $PM_{2.5}$ measurements. Two stations in central Georgia measured high $PM_{2.5}$ at 12Z. These measurements probably contribute to the slightly increased $PM_{2.5}$ at 18Z in the surrounding region. However, they did not lead to any high $PM_{2.5}$ values at 18Z that were measured by several stations in the region. When both AOD and AirNow observations are assimilated, the $PM_{2.5}$ results of C3 at 18Z resemble case C1. These results are particularly affected by the fact that all aerosol components were adjusted according to Terra AOD just 1 h before, at 17Z. The effect of the $PM_{2.5}$ integration at 12Z is hardly noticeable after 6 h. In an area with dense AirNow station distribution, such as in the San Francisco Bay Area, improvement of case C3 over case C1 can be detected.

Figure 7 shows that C1 and C3 predicted a peak mean 24 h average $PM_{2.5}$ in the Northeast region on 20 July, while the AirNow surface observations show a peak on the next day with a lower value. This day is chosen to demonstrate that assimilating AOD using the current approach can lead to large errors in certain circumstances. High AOD were observed by both Terra and Aqua mainly over Ontario, Canada, and upper New York state on 19 July, as shown in Figure 8. On 20 July, the high AODs are mostly in Quebec, Canada, and the New England area of the U.S. However, most AirNow stations in the Northeast region only recorded moderate $PM_{2.5}$ readings at 06Z, 12Z, and 18Z on 20 July, while high $PM_{2.5}$ were observed at several scattered locations (see Figures 9 and 11). As a result, the integration of the AOD observations generated a large overestimation of surface $PM_{2.5}$ by C1 and C3 in a large portion of the NE region, as shown in Figure 11. The observed high AOD values were caused by smoke plumes originating from the wildfires over northwestern Ontario occurring between 17 and 19 July 2011 [*Palmer et al.*, 2013; *Griffin et al.*, 2013; *Franklin et al.*, 2014; *Sofowote and Dempsey*, 2015]. It is likely that the biomass emitted from the wildfires was injected into the upper troposphere and stayed aloft during transport. Thus, the event well captured by the MODIS instruments was not detected by the ground instruments until further downwind. In such events, assigning the observed AOD uniformly throughout the vertical column caused a large overestimation of surface $PM_{2.5}$

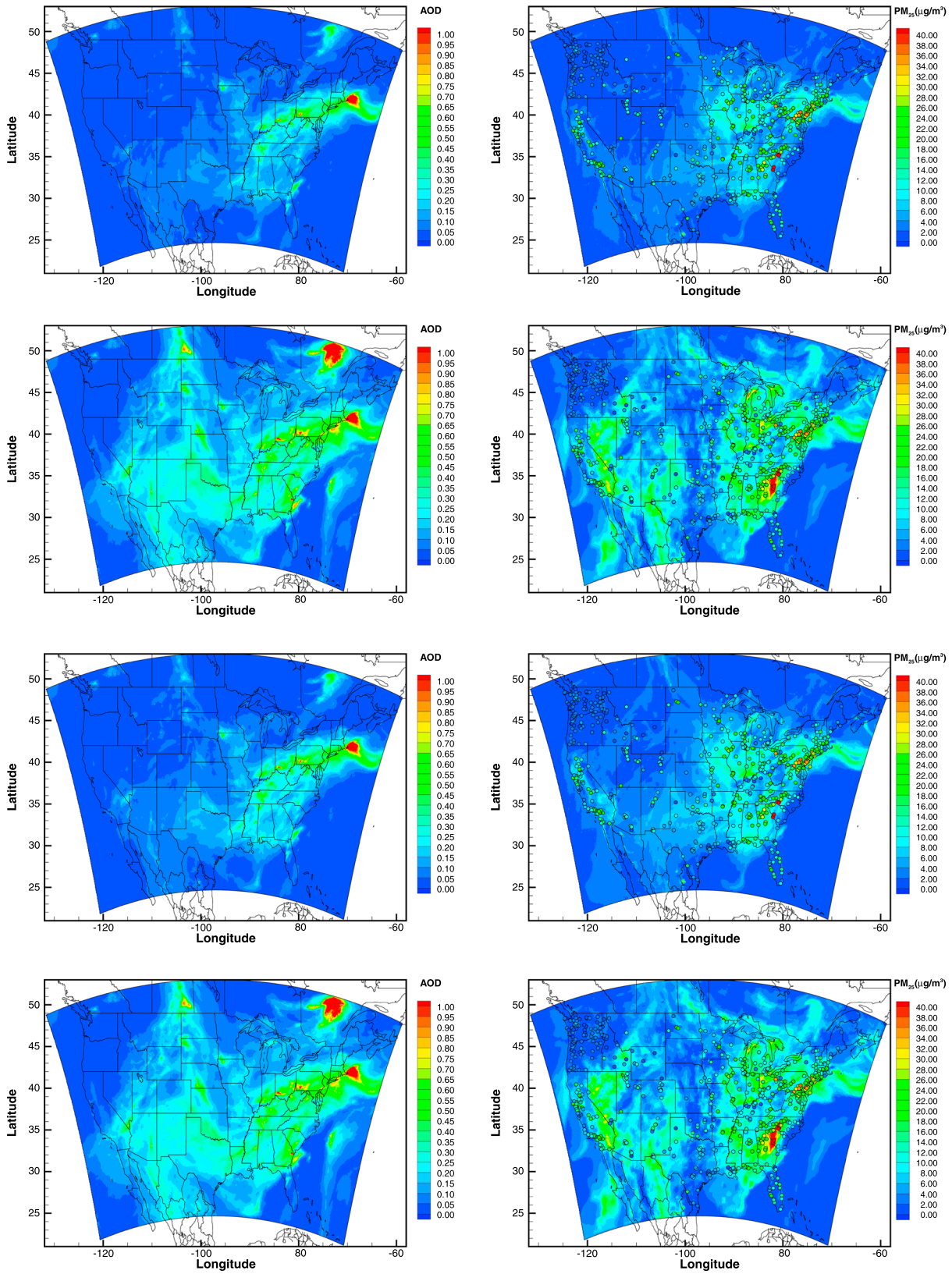

Figure 10. CMAQ simulated (left column) AOD and (right column) surface $PM_{2.5}$ of cases C0-3 (top to bottom) on 8 July 2011. AirNow stations are shown as circles, and the measurement values are indicated by the filling color following the same code as the $PM_{2.5}$ contours.

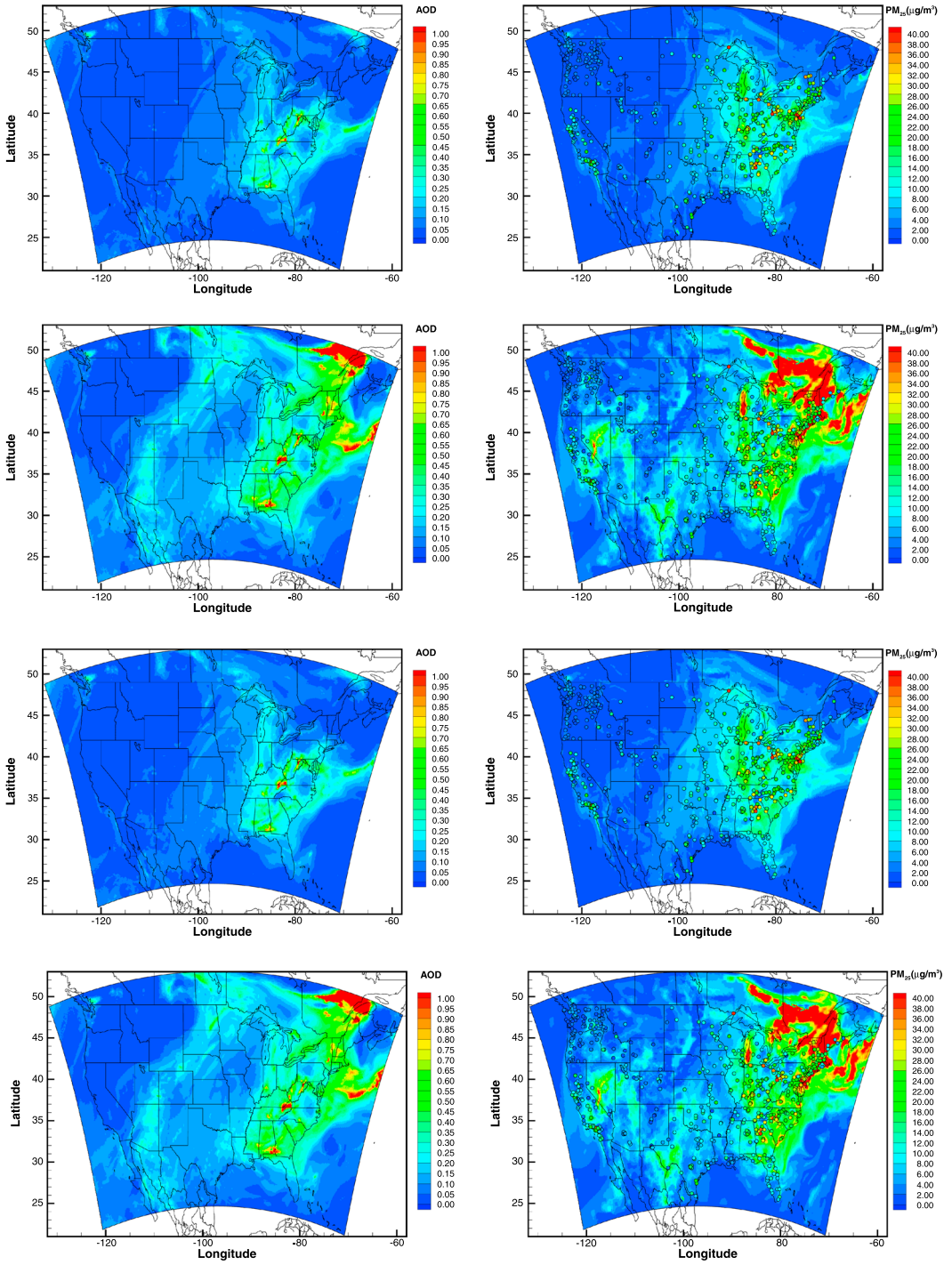

Figure 11. CMAQ simulated (left column) AOD and (right column) surface $PM_{2.5}$ of cases C0-3 (top to bottom) on 20 July 2011. AirNow stations are shown as circles, and the measurement values are indicated by the filling color following the same code as the $PM_{2.5}$ contours.

in cases C1 and C3 here. When there are $PM_{2.5}$ measurements around the AOD observations, *Tang et al.* [2015] limited the aerosol adjustment based on AOD assimilation to the region above the boundary layer. This approach is considered a little arbitrary and not adopted here. The distribution of the airborne mass indicated by AOD observations can be assisted by a smoke-plume model, especially when the sources are well known. For instance, *Sofowote and Dempsey* [2015] used the Hybrid Single Particle Lagrangian Integrated Trajectory (HYSPLIT) model [*Draxler and Hess*, 1998] and the NOAA's Global Data Assimilation System (GDAS)

[*Kleist et al.*, 2009] meteorological data to investigate this exact event, explaining the high $PM_{2.5}$ episodes observed at five surface stations in southeast Canada.

Other than in the Northeast region, the assimilation of AOD observations proves to be beneficial, especially in the Southeast region. In Figure 8, both Aqua on 19 July and Terra on 20 July show high AODs in the Southeast region. These are quite consistent with the surface $PM_{2.5}$ measurements at 12Z and 18Z on 20 July shown in Figures 9 and 11, respectively. AOD assimilation helps cases C1 and C3 generate $PM_{2.5}$ better matching the AirNow observations in these regions at 18Z on 20 July 2011, as shown in Figure 11. With only $PM_{2.5}$ assimilated, C2 changes little over the baseline case. Underestimation is slightly mitigated in southern California, Lake Michigan, and on the border between Virginia and North Carolina. Similarly to 8 July, case C3 here is almost indistinguishable from C1. There are still some noticeable changes, such as the reduced $PM_{2.5}$ in upper Lake Michigan in case C3.

4. Summary and Discussion

Using a simple optimal interpolation method, the MODIS AOD and AirNow $PM_{2.5}$ measurements were assimilated into the CMAQ model over a 30 day test period in July 2011. The results show that assimilating either the MODIS AOD or the AirNow $PM_{2.5}$ helps $PM_{2.5}$ predictions over the entire 30 days, with the configuration that assimilates observations from both sources achieving the best results as measured by the daily averaged and domain-averaged biases and RMSEs calculated using the unassimilated or not-yet-assimilated AirNow $PM_{2.5}$ observations. For the test period, assimilating total AOD observations proves to be more beneficial in correcting the $PM_{2.5}$ underestimations than assimilating the AirNow $PM_{2.5}$ measurements directly. This is consistent with the results presented by *Schwartz et al.* [2012] using WRF-Chem model and 3DVAR method over the CONUS for a 44 day summer period in 2010. The better spatial coverage of the MODIS AOD observations is probably the main reason for its larger effect in the assimilation tests.

The simple approach of applying AOD scaling factors uniformly throughout the vertical column proves very effective most of the time during the test period. However, some high-AOD events are caused by aerosols in the middle of the air column, such as smoke plumes resulting from certain large wildfires. In such cases, distributing the observed air mass vertically according to the original model's vertical profile is invalid and will substantially overestimate surface $PM_{2.5}$. This is demonstrated by the high-AOD event in the Northeast U.S. that was caused by the widespread wildfires in northwestern Ontario between 17 and 19 July 2011. When the source locations are known, a separate Lagrangian dispersion model, such as the HYSPLIT model, can help better define the vertical distribution of the unaccounted aerosol mass detected by space-borne instruments.

In the current method, the composition of aerosol species is kept intact. The modification of the various aerosol species using a single scaling factor was chosen for its simplicity. However, it is possible to adjust the aerosol species differently using their respective Jacobian components. *Liu et al.* [2011] adjusted the concentration of 14 aerosol variables from the Goddard Chemistry Aerosol Radiation and Transport (GOCART) model by assimilating the MODIS AOD observations and then initialized the Weather Research and Forecasting/Chemistry (WRF/Chem) model for improved aerosol analyses and forecasts. However, such a practice may risk introducing too many degrees of freedom to the unknowns that are difficult to determine without the ready availability of additional observations of the aerosol components.

The current procedure improves $PM_{2.5}$ predictions by modifying the state variables. Although the model "forecast" periods are no more than 21 h before assimilating newly available data, accumulative impacts of the assimilation on the forecast are clearly shown. Throughout the entire procedure, the key model parameters and the emission sources are unchanged. While this allows the assimilation scheme to be flexible and allows the model to be modified independently, it suffers the drawback of freely grown model errors due to inherent deficiencies. Among the sources of model error, the emission terms derived from the often outdated emission inventories may be the most uncertain. These can certainly benefit from being constrained by the observations. For instance, the exaggerated diurnal profiles shown by the CMAQ $PM_{2.5}$ results are likely caused by temporal profiles of the emission sources, PBL height, or removal processes and cannot be corrected by the assimilation scheme implemented here. *Tong et al.* [2012] discussed a promising future improvement to the aerosol forecasts that could be achieved by adjusting the emission terms using the observations. In this study, the error statistics are kept constant without temporal or spatial variations. *Tang et al.* [2015] applied

"dynamic uncertainties" and showed improvement over the constant statistics. Implementing more realistic error statistics will be explored. Assimilating MODIS observed radiance instead of AOD data has also been shown to be promising [*Xu et al.*, 2013] and will be investigated in the future.

Acknowledgments
This study was supported by NOAA grant NA09NES4400006 (Cooperative Institute for Climate and Satellites-CICS) at the NOAA Air Resources Laboratory in collaboration with the University of Maryland. MODIS AOD data are available at modis-atmos.gsfc.nasa.gov/MOD04_L2/. To access the AirNow $PM_{2.5}$ measurements, please submit request via airnowapi.org.

References

Adhikary, B., et al. (2008), A regional scale chemical transport modeling of Asian aerosols with data assimilation of AOD observations using optimal interpolation technique, *Atmos. Environ.*, *42*(37), 8600–8615, doi:10.1016/j.atmosenv.2008.08.031.

Baek, J., Y. Hu, M. T. Odman, and A. G. Russell (2011), Modeling secondary organic aerosol in CMAQ using multigenerational oxidation of semi-volatile organic compounds, *J. Geophys. Res.*, *116*, D22204, doi:10.1029/2011JD015911.

Bocquet, M., et al. (2015), Data assimilation in atmospheric chemistry models: Current status and future prospects for coupled chemistry meteorology models, *Atmos. Chem. Phys.*, *15*(10), 5325–5358, doi:10.5194/acp-15-5325-2015.

Byun, D., and K. L. Schere (2006), Review of the governing equations, computational algorithms, and other components of the Models-3 Community Multiscale Air Quality (CMAQ) modeling system, *Appl. Mech. Rev.*, *59*(56), 51–77.

Carlton, A. G., P. V. Bhave, S. L. Napelenok, E. D. Edney, G. Sarwar, R. W. Pinder, G. A. Pouliot, and M. Houyoux (2010), Model representation of secondary organic aerosol in CMAQv4.7, *Environ. Sci. Technol.*, *44*(22), 8553–8560, doi:10.1021/es100636q.

Carmichael, G. R., A. Sandu, T. Chai, D. N. Daescu, E. M. Constantinescu, and Y. Tang (2008), Predicting air quality: Improvements through advanced methods to integrate models and measurements, *J. Comput. Phys.*, *227*(7), 3540–3571, doi:10.1016/j.jcp.2007.02.024.

Chai, T., et al. (2007), Four-dimensional data assimilation experiments with International Consortium for Atmospheric Research on Transport and Transformation ozone measurements, *J. Geophys. Res.*, *112*, D12S15, doi:10.1029/2006JD007763.

Chai, T., G. R. Carmichael, Y. Tang, A. Sandu, A. Heckel, A. Richter, and J. P. Burrows (2009), Regional NO_x emission inversion through a four-dimensional variational approach using SCIAMACHY tropospheric NO_2 column observations, *Atmos. Environ.*, *43*(32), 5046–5055.

Chai, T., et al. (2013), Evaluation of the United States National Air Quality Forecast Capability experimental real-time predictions in 2010 using Air Quality System ozone and NO_2 measurements, *Geosci. Model Dev.*, *6*(5), 1831–1850, doi:10.5194/gmd-6-1831-2013.

Chai, T., P. Lee, L. Pan, H. Kim, and D. Tong (2014), Building and testing atmospheric chemistry reanalysis modeling system, in *Air Pollution Modeling and Its Application XXIII*, edited by D. Steyn and R. Mathur, pp. 581–585, Springer Int. Publ., Switzerland, doi:10.1007/978-3-319-04379-1_96.

Chai, T., A. Crawford, B. Stunder, M. J. Pavolonis, R. Draxler, and A. Stein (2017), Improving volcanic ash predictions with the HYSPLIT dispersion model by assimilating MODIS satellite retrievals, *Atmos. Chem. Phys.*, *17*(4), 2865–2879, doi:10.5194/acp-17-2865-2017.

Chow, J., J. Watson, H. Kuhns, V. Etyemezian, D. Lowenthal, D. Crow, S. Kohl, J. Engelbrecht, and M. Green (2004), Source profiles for industrial, mobile, and area sources in the Big Bend Regional Aerosol Visibility and Observational Study, *Chemosphere*, *54*(2), 185–208, doi:10.1016/j.chemosphere.2003.07.004.

Dee, D., and A. Da Silva (1998), Data assimilation in the presence of forecast bias, *Q. J. R. Meteorol. Soc.*, *124*(545, A), 269–295, doi:10.1002/qj.49712454512.

Dee, D. P. (2005), Bias and data assimilation, *Q. J. R. Meteorol. Soc.*, *131*(613, C), 3323–3343, doi:10.1256/qj.05.137.

Delfino, R., C. Sioutas, and S. Malik (2005), Potential role of ultrafine particles in associations between airborne particle mass and cardiovascular health, *Environ. Health. Persp.*, *113*(8), 934–946, doi:10.1289/ehp.7938.

Djalalova, I., L. Delle Monache, and J. Wilczak (2015), PM2.5 analog forecast and Kalman filter post-processing for the Community Multiscale Air Quality (CMAQ) model, *Atmos. Environ.*, *108*, 76–87, doi:10.1016/j.atmosenv.2015.02.021.

Dominici, F., R. Peng, M. Bell, L. Pham, A. McDermott, S. Zeger, and J. Samet (2006), Fine particulate air pollution and hospital admission for cardiovascular and respiratory diseases, *J. Am. Med. Assoc.*, *295*(10), 1127–1134.

Doraiswamy, P., C. Hogrefe, W. Hao, K. Civerolo, J.-Y. Ku, and G. Sistla (2010), A retrospective comparison of model-based forecasted $PM_{2.5}$ concentrations with measurements, *J. Air Waste Manage. Assoc.*, *60*(11), 1293–1308, doi:10.3155/1047-3289.60.11.1293.

Draxler, R., and G. Hess (1998), An overview of the HYSPLIT_4 modeling system for trajectories, dispersion and deposition, *Aust. Meteorol. Mag.*, *47*(4), 295–308.

Drury, E., D. J. Jacob, J. Wang, R. J. D. Spurr, and K. Chance (2008), Improved algorithm for MODIS satellite retrievals of aerosol optical depths over western North America, *J. Geophys. Res.*, *113*, D16204, doi:10.1029/2007JD009573.

Franklin, J. E., et al. (2014), A case study of aerosol scavenging in a biomass burning plume over eastern Canada during the 2011 BORTAS field experiment, *Atmos. Chem. Phys.*, *14*(16), 8449–8460, doi:10.5194/acp-14-8449-2014.

Gorline, J. L., and P. Lee (2009), Performance evaluation of NOAA-EPA developmental aerosol forecasts, *Environ. Fluid Mech.*, *9*, 109–120.

Griffin, D., et al. (2013), Investigation of CO, C_2H_6 and aerosols in a boreal fire plume over eastern Canada during BORTAS 2011 using ground- and satellite-based observations and model simulations, *Atmos. Chem. Phys.*, *13*(20), 10,227–10,241, doi:10.5194/acp-13-10227-2013.

Holben, B., et al. (1998), AERONET—A federated instrument network and data archive for aerosol characterization, *Remote Sens. Environ.*, *66*(1), 1–16, doi:10.1016/S0034-4257(98)00031-5.

Hyer, E. J., J. S. Reid, and J. Zhang (2011), An over-land aerosol optical depth data set for data assimilation by filtering, correction, and aggregation of MODIS Collection 5 optical depth retrievals, *Atmos. Meas. Tech.*, *4*(3), 379–408, doi:10.5194/amt-4-379-2011.

Janjic, Z. I. (2003), A nonhydrostatic model based on a new approach, *Meteorol. Atmos. Phys.*, *82*, 271–285, doi:10.1007/s00703-001-0587-6.

Kaiser, J. W., et al. (2012), Biomass burning emissions estimated with a global fire assimilation system based on observed fire radiative power, *Biogeosciences*, *9*(1), 527–554, doi:10.5194/bg-9-527-2012.

Kang, D., R. Mathur, and S. T. Rao (2010a), Real-time bias-adjusted O_3 and PM2.5 air quality index forecasts and their performance evaluations over the continental United States, *Atmos. Environ.*, *44*(18), 2203–2212, doi:10.1016/j.atmosenv.2010.03.017.

Kang, D., R. Mathur, and S. T. Rao (2010b), Assessment of bias-adjusted PM2.5 air quality forecasts over the continental United States during 2007, *Geosci. Model Dev.*, *3*(1), 309–320.

Kleist, D. T., D. F. Parrish, J. C. Derber, R. Treadon, W.-S. Wu, and S. Lord (2009), Introduction of the GSI into the NCEP Global Data Assimilation System, *Weather Forecasting*, *24*(6), 1691–1705, doi:10.1175/2009WAF2222201.1.

Lee, P., and F. Ngan (2011), Coupling of important physical processes in the planetary boundary layer between meteorological and chemistry models for regional to continental scale air quality forecasting: An overview, *Atmosphere*, *2*, 464–483.

Lee, P., et al. (2017), NAQFC developmental forecast guidance for fine particulate matter (PM2.5), *Weather Forecasting*, *32*(1), 343–360, doi:10.1175/WAF-D-15-0163.1.

Levy, R. C., L. A. Remer, D. Tanré, S. Mattoo, and Y. J. Kaufman (2009), Algorithm for remote sensing of tropospheric aerosol over dark targets from MODIS: Collections 005 and 051, NASA Goddard Space Flight Center, Greenbelt, Md. [Available at http://modis-atmos.gsfc.nasa.gov/_docs/ATBD_MOD04_C005_rev2.pdf, revision2.]

Levy, R. C., S. Mattoo, L. A. Munchak, L. A. Remer, A. M. Sayer, F. Patadia, and N. C. Hsu (2013), The Collection 6 MODIS aerosol products over land and ocean, *Atmos. Meas. Tech.*, *6*(11), 2989–3034, doi:10.5194/amt-6-2989-2013.

Liu, Z., Q. Liu, H.-C. Lin, C. S. Schwartz, Y.-H. Lee, and T. Wang (2011), Three-dimensional variational assimilation of MODIS aerosol optical depth: Implementation and application to a dust storm over East Asia, *J. Geophys. Res.*, *116*, D23206, doi:10.1029/2011JD016159.

Luo, C., Y. Wang, S. Mueller, and E. Knipping (2011), Diagnosis of an underestimation of summertime sulfate using the Community Multiscale Air Quality model, *Atmos. Environ.*, *45*(29), 5119–5130, doi:10.1016/j.atmosenv.2011.06.029.

McKeen, S., et al. (2007), Evaluation of several $PM_{2.5}$ forecast models using data collected during the ICARTT/NEAQS 2004 field study, *J. Geophys. Res.*, *112*, D10S20, doi:10.1029/2006JD007608.

Mebust, M., B. Eder, F. Binkowski, and S. Roselle (2003), Models-3 Community Multiscale Air Quality (CMAQ) model aerosol component 2. Model evaluation, *J. Geophys. Res.*, *108*(D6), 4184, doi:10.1029/2001JD001410.

Morris, R., B. Koo, and G. Yarwood (2005a), Evaluation of multisectional and two-section particulate matter photochemical grid models in the western United States, *J. Air Waste Manage. Assoc.*, *55*(11), 1683–1693.

Morris, R., D. McNally, T. Tesche, G. Tonnesen, J. Boylan, and P. Brewer (2005b), Preliminary evaluation of the community multiscale air, quality model for 2002 over the southeastern United States, *J. Air Waste Manage. Assoc.*, *55*(11), 1694–1708.

Morris, R. E., B. Koo, A. Guenther, G. Yarwood, D. McNally, T. W. Tesche, G. Tonnesen, J. Boylan, and P. Brewer (2006), Model sensitivity evaluation for organic carbon using two multi-pollutant air quality models that simulate regional haze in the southeastern United States, *Atmos. Environ.*, *40*(26), 4960–4972, doi:10.1016/j.atmonsenv.2005.09.088.

Otte, T. L., et al. (2005), Linking the Eta model with the Community Multiscale Air Quality (CMAQ) modeling system to build a national air quality forecasting system, *Weather Forecasting*, *20*, 367–384, doi:10.1175/WAF855.1.

Pagowski, M., Z. Liu, G. A. Grell, M. Hu, H. C. Lin, and C. S. Schwartz (2014), Implementation of aerosol assimilation in Gridpoint Statistical Interpolation (v. 3.2) and WRF-Chem (v. 3.4.1), *Geosci. Model Dev.*, *7*(4), 1621–1627, doi:10.5194/gmd-7-1621-2014.

Palmer, P. I., et al. (2013), Quantifying the impact of BOReal forest fires on Tropospheric oxidants over the Atlantic using Aircraft and Satellites (BORTAS) experiment: Design, execution and science overview, *Atmos. Chem. Phys.*, *13*(13), 6239–6261, doi:10.5194/acp-13-6239-2013.

Pan, L., D. Tong, P. Lee, H. C. Kim, and T. Chai (2014), Assessment of NO_x and O_3 forecasting performances in the US National Air Quality Forecasting Capability before and after the 2012 major emissions updates, *Atmos. Environ.*, *95*, 610–619, doi:10.1016/j.atmosenv.2014.06.020.

Remer, L., et al. (2005), The MODIS aerosol algorithm, products, and validation, *J. Atmos. Sci.*, *62*(4), 947–973.

Robichaud, A., and R. Ménard (2014), Multi-year objective analyses of warm season ground-level ozone and $PM_{2.5}$ over North America using real-time observations and Canadian operational air quality models, *Atmos. Chem. Phys.*, *14*(4), 1769–1800, doi:10.5194/acp-14-1769-2014.

Saide, P. E., G. R. Carmichael, Z. Liu, C. S. Schwartz, H. C. Lin, A. M. da Silva, and E. Hyer (2013), Aerosol optical depth assimilation for a size-resolved sectional model: Impacts of observationally constrained, multi-wavelength and fine mode retrievals on regional scale analyses and forecasts, *Atmos. Chem. Phys.*, *13*(20), 10,425–10,444, doi:10.5194/acp-13-10425-2013.

Sandu, A., and T. Chai (2011), Chemical data assimilation—An overview, *Atmosphere*, *2*(3), 426–463, doi:10.3390/atmos2030426.

Schwartz, C. S., Z. Liu, H.-C. Lin, and S. A. McKeen (2012), Simultaneous three-dimensional variational assimilation of surface fine particulate matter and MODIS aerosol optical depth, *J. Geophys. Res.*, *117*, D13202, doi:10.1029/2011JD017383.

Schwartz, J., and L. Neas (2000), Fine particles are more strongly associated than coarse particles with acute respiratory health effects in schoolchildren, *Epidemiology*, *11*(1), 6–10, doi:10.1097/00001648-200001000-00004.

Schwede, D., G. Pouliot, and T. Pierce (2005), Changes to the biogenic emissions inventory system version 3 (BEIS3), paper presented at 4th Annual CMAS Models-3 User's Conference, CMAS Cent., Chapel Hill, NC, 26–28 Sept.

Seidel, D. J., and A. N. Birnbaum (2015), Effects of independence day fireworks on atmospheric concentrations of fine particulate matter in the United States, *Atmos. Environ.*, *115*, 192–198.

Sofowote, U., and F. Dempsey (2015), Impacts of forest fires on ambient near-real-time PM2.5 in Ontario, Canada: Meteorological analyses and source apportionment of the July 2011-2013 episodes, *Atmos. Pollut. Res.*, *6*(1), 1–10, doi:10.5094/APR.2015.001.

Sun, Y., G. Zhuang, A. Tang, Y. Wang, and Z. An (2006), Chemical characteristics of PM2.5 and PM10 in haze-fog episodes in Beijing, *Environ. Sci. Technol.*, *40*(10), 3148–3155, doi:10.1021/es051533g.

Tang, Y., T. Chai, L. Pan, P. Lee, D. Tong, H.-C. Kim, and W. Chen (2015), Using optimal interpolation to assimilate surface measurements and satellite AOD for ozone and $PM_{2.5}$: A case study for July 2011, *J. Air Waste Manage. Assoc.*, *65*(10), 1206–1216, doi:10.1080/10962247.2015.1062439.

Tong, D., P. Lee, and R. Saylor (2012), New directions: The need to develop process-based emission forecasting, *Atmos. Environ.*, *47*, 560–561, doi:10.1016/j.atmosenv.2011.10.070.

Wang, J., X. Xu, R. Spurr, Y. Wang, and E. Drury (2010), Improved algorithm for MODIS satellite retrievals of aerosol optical thickness over land in dusty atmosphere: Implications for air quality monitoring in china, *Remote Sens. Environ.*, *114*(11), 2575–2583, doi:10.1016/j.rse.2010.05.034.

Wang, Y., J. Wang, X. Xu, D. K. Henze, Y. Wang, and Z. Qu (2016), A new approach for monthly updates of anthropogenic sulfur dioxide emissions from space: Application to China and implications for air quality forecasts, *Geophys. Res. Lett.*, *43*, 9931–9938, doi:10.1002/2016GL070204.

Xing, J., R. Mathur, J. Pleim, C. Hogrefe, C.-M. Gan, D. C. Wong, C. Wei, R. Gilliam, and G. Pouliot (2015), Observations and modeling of air quality trends over 1990–2010 across the Northern Hemisphere: China, the United States and Europe, *Atmos. Chem. Phys.*, *15*(5), 2723–2747, doi:10.5194/acp-15-2723-2015.

Xu, X., J. Wang, D. K. Henze, W. Qu, and M. Kopacz (2013), Constraints on aerosol sources using GEOS-Chem adjoint and MODIS radiances, and evaluation with multisensor (OMI, MISR) data, *J. Geophys. Res. Atmos.*, *118*(12), 6396–6413, doi:10.1002/jgrd.50515.

Zhang, J., and J. S. Reid (2006), MODIS aerosol product analysis for data assimilation: Assessment of over-ocean level 2 aerosol optical thickness retrievals, *J. Geophys. Res.*, *111*, D22207, doi:10.1029/2005JD006898.

Zhang, J., J. S. Reid, D. L. Westphal, N. L. Baker, and E. J. Hyer (2008), A system for operational aerosol optical depth data assimilation over global oceans, *J. Geophys. Res.*, *113*, D10208, doi:10.1029/2007JD009065.

Zhang, L., et al. (2015), Constraining black carbon aerosol over Asia using OMI aerosol absorption optical depth and the adjoint of GEOS-Chem, *Atmos. Chem. Phys.*, *15*(18), 10,281–10,308, doi:10.5194/acp-15-10281-2015.